Optica Applicata, Vol. LII, No. 3, 2022
DOI: 10.37190/oa220308

Abruptly autofocusing property of circular Pearcey vortex beams with different initial launch angles in harmonic potentials

Xianglian Liu*, Di Zhang, Lijiao Zhao, Pu Li, Jianguo Zhang, Yi Liu

Key Laboratory of Advanced Transducers and Intelligent Control System, Ministry of Education, College of Physics and Optoelectronics, Taiyuan University of Technology, Taiyuan, Shanxi, 030024, China

*Corresponding author: liuxianglian@tyut.edu.cn

We have studied and explored the influence of different launch angles on the circular Pearcey beams (CPBs) without vortex or with vortex for the first time. Although launch angles can manipulate the focal length and the contrast of peak intensity of the CPBs, the shape and propagation trajectory of the CPBs maintain invariant. When the vortex is considered, the focal pattern and the contrast of peak intensity of the circular Pearcey vortex beams (CPVBs) can be changed by adjusting the magnitude of topological charges and the position of vortex. In addition, we have deliberated the propagation of the CPVBs under the action of double opposite optical vortices.

Keywords: autofocusing beam, optical vortices, Pearcey.

1. Introduction

Abruptly autofocusing (AAF) beams, which can suddenly focus all their energy in the whole propagation process without the lens and nonlinearity, can maintain a relatively low intensity up to the focal point. These fascinating properties have been studied both analytically [1] and numerically [2, 3]. Due to these novel properties, the AAF beams are the ideal candidates for the laser biomedical treatment [1], microparticle manipulation [3], multiphoton polymerization [4], and high-power terahertz generation [5]. As is well known, the Airy beams [6] and Bessel beams [7] are a part of typical abruptly autofocusing beams. Their characteristics have been widely discussed [8–13].

The optical vortices (OVs) have attracted lots of attention due to the fascinating features in the past few years. The OVs possess an optical singularity at the optical center owing to phase modulation, which shows the structure of cylindrical symmetry in the process of transmission. The OVs carry the orbital angular momentum (OAM) and the light intensity at the center is zero. The phase distribution of the OVs is spiral, which is determined by the topological charge. The wave vector has an azimuth angle, and it revolves around the center of the vortex so it is immensely meaningful to apply

the domain of optical tweezers technology [14] and optical communication [15]. Recently, the fantastic characteristics of OVs applied in diverse beams have been widely studied. For instance, Airy beams added OVs have been researched in 2012 [16, 17]. Airy–Gaussian beams with OVs also have been discussed in 2015 [18].

Recently, RING *et al*. have produced limited energy Pearcey beam experimentally compared to previous theoretical research, and Pearcey function was first introduced into optical system in 2012 [19]. Since then, the properties of Pearcey beams have been extensively discussed by other researchers. In 2013, DENG *et al*. have discussed the virtual light source of Pearcey beams [20]. In 2015, KOVALEV *et al*. have obtained the half-Pearcey beam from the paraxial Helmholtz equation, and emphasized that the Pearcey beam can be composed by the interference of two half-Pearcey beams [21]. It is worth mentioning that CHEN *et al*. have first explored the circular Pearcey beams in 2018 [22]. The distinguishing feature of circular Pearcey beam can enhance the peak intensity and shorten the focal length compared with circular Airy beams. In order to increase the peak intensity contrast, alter the locations of the focal point, and transform the focal pattern, the properties of Pearcey beams under different conditions have been studied, such as circular Pearcey vortex beam with chirp, second-order chirp, harmonic potential, parabolic refractive index [23–26] and so on. The results of research manifest that the launch angle is a significant parameter for Airy beams to control the focal length and the peak intensity contrast [27, 28]. Nevertheless, how different launch angles affect the properties of the CPVBs is still unexplored. In this paper, we will discuss how different launch angles affect the properties of the CPVBs by adopting the fast split-step Fourier method [29, 30].

Numerical simulations show that different launch angles can be used to modulate the focal intensity and focal position. The decline of focal length accompanies the enhancement of the peak intensity contrast of the CPBs when increasing the value of angles if the launch angle is positive. In contrast, when the launch angle is negative, as the value of absolute angle increases, the focal length ascends while the peak intensity contrast descends. However, the launch angle does not change the intensity of initial plane and the propagation trajectory of the CPBs. In addition, we also have studied the variation of the CPVBs by adjusting the magnitude of topological charges as well as the position of vortex under a fixed launch angle, which can alter the peak intensity contrast and focal pattern. Finally, the autofocusing properties of the CPVBs with two opposite vortices have been investigated.

2. The theoretical model

The propagation dynamics of the CPVBs under a harmonic potential is governed by the (2 + 1) dimensional Schrödinger equation, which can be described as [31]:

$$\frac{\partial^2}{\partial x^2}E + \frac{\partial^2}{\partial y^2}E + 2i\frac{\partial}{\partial z}E - \alpha(x^2 + y^2)E = 0 \tag{1}$$

where E is the envelope of optical beam, Variables $x(y)$ and z represent normalized transverse coordinates and propagation distances, which are scaled by a transverse width x_0 and Rayleigh range kx_0^2, respectively, $k = 2\pi n/\lambda_0$ is the wave number, λ_0 is the wavelength in free space, n is the refractive index. Parameter α of the last term of formula (1) can control the width of harmonic potential. With the purpose of describing the propagation properties of the CPVBs conveniently, the formula (1) can be rewritten in polar coordinates, which is described as:

$$\frac{\partial^2}{\partial r^2}E + r^{-1}\frac{\partial}{\partial r}E + r^{-2}\frac{\partial^2}{\partial \varphi^2}E + 2i\frac{\partial}{\partial z}E - \alpha^2 r^2 E = 0 \tag{2}$$

In formula (2), $\varphi = \arctan(y/x)$ represents the azimuthal angle, $r = \sqrt{x^2 + y^2}$ is the radial coordinate. The electric fields for the CPVBs under different initial launch angles v (or "velocity") can be described as

$$E(r, \varphi, 0) = \begin{cases} A_0 \mathrm{Pe}\left(-\dfrac{r}{\mu}, -\dfrac{r}{\beta}\right)\exp(-r^2)\exp(ar^b)\exp(ivr) \\ \quad \times \left[r\exp(i\varphi) + k\exp(i\varphi_k)\right]^m \left[r\exp(i\varphi) - k\exp(i\varphi_k)\right]^n, & r > r_0 \\ 0, & r < r_0 \end{cases} \tag{3}$$

where A_0 is the amplitude of the electric fields. The initial velocity of CPVBs is related to the incident angle θ, so that the accelerating properties of CPVBs can be controlled by θ, which can be written as $\theta = \arcsin(v/x_0 k)$, such as $(v = \pm 5) \leftrightarrow (\theta = \pm 0.1887°)$; β is the scaled parameter. What we need to emphasize is that parameter μ is the spatial distribution factor which can dramatically change the properties of CPVBs, (m, n) and (k, φ_k) denote the topological charges and position of the OVs. Pe$(\cdot)$ is the abbreviation of the Pearcey integral [32], and the definition of the Pearce integral function is

$$\mathrm{Pe}(X, Y) = \int_R \exp\left[i(s^4 + sX + s^2 Y)\right]\mathrm{d}s \tag{4}$$

We insert the incident electric field of Eq. (3) into the polar coordinate Eq. (2). Using the Fresnel integral, the solution can be described as

$$E(r, \varphi, z) = \int_0^{2\pi}\int_0^{\infty} \frac{E(\rho, \theta, 0)}{2\pi i z}\exp\left[i\frac{\rho^2 + r^2 - 2\rho r\cos(\varphi - \theta)}{2z}\right]\rho\,\mathrm{d}\rho\,\mathrm{d}\theta \tag{5}$$

It is difficult to obtain the exact solution of the nonlinear Schrodinger equation, so we apply the fast split-step Fourier method to obtain the analytical solution for Eq. (5) [29, 30]. The parameters we chose are as follows: $A_0 = 1$, $\alpha = 0.5$, $\mu = 0.1$, $\beta = 0.1$,

$m = 0$, $n = 0$, $x_0 = 100$ μm, $\lambda = 533$ nm, $a = 0.1$, $b = 1$, and $r_0 = 1.5$. When different parameters are chosen it is indicated by corresponding notes.

3. Discussions and analyses

3.1. The properties of the CPBs with different launch angles

Firstly, we simulate the evolution of the CPBs with different propagation distances as well as the influence of different launch angles on the focal intensity and focal length of the CPBs. Figure 1(**a1**) describes the intensity distribution of the initial plane of the CPBs without the launch angles, which has a symmetrical doughnut shape. With

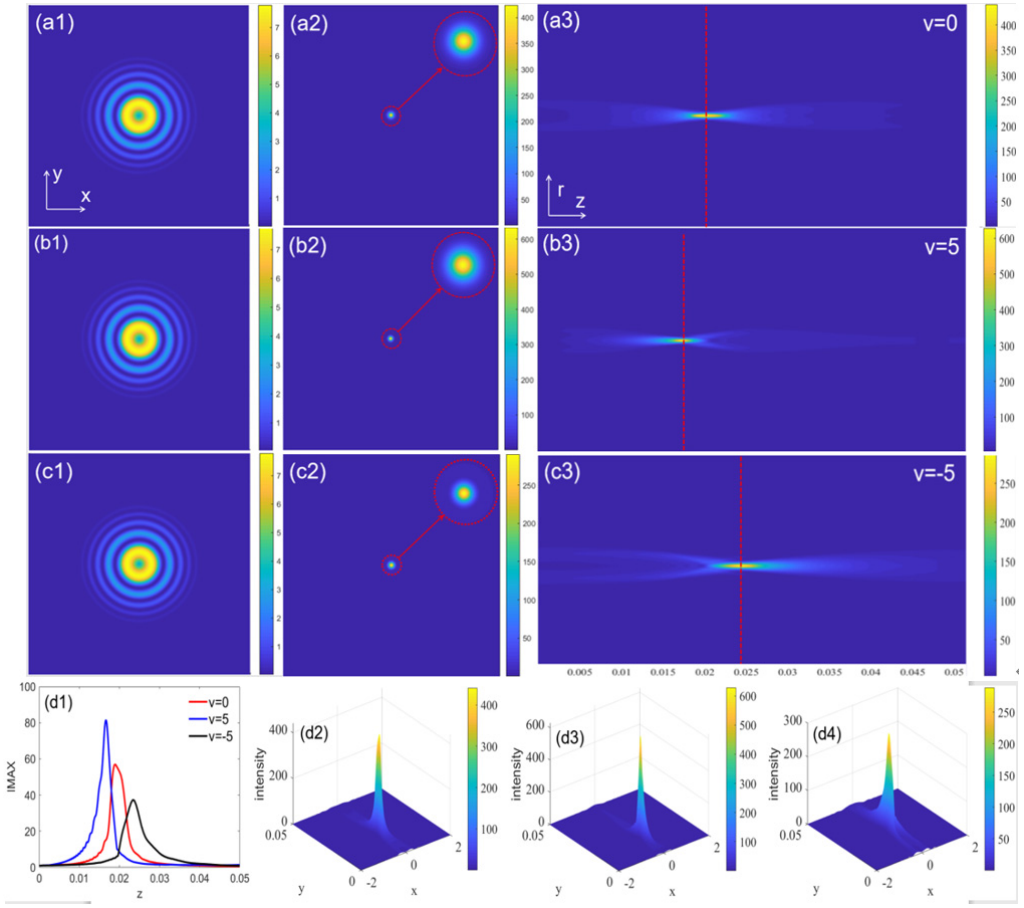

Fig. 1. The evolutions of the CPBs with different launch angles in the process of transmission: (**a**) $v = 0$, (**b**) $v = 5$, (**c**) $v = -5$. (**a1**)–(**c1**) the shape and intensity distribution of the initial plane. (**a2**)–(**c2**) the shape and intensity distribution of the focal plane. (**a3**)–(**c3**) the side-view intensity profiles of the CPBs. The red dotted lines of (**a3**)–(**c3**) indicate the positions of the focus point. (**d1**) The intensity profile of IMAX and focal length of the CPBs for $v = 0$, 5, –5, respectively. The three-dimensional maps of the intensity distribution with different launch angles v are depicted in (**d2**)–(**d3**).

increasing the propagation distance, the dimension of the CPBs is lessened while the peak intensity is increased gradually. The peak intensity reaches the highest when the propagation distance approaches the focal point as shown in Fig. 1(**a2**). The side-view intensity profile of the CPBs in the process of transmission is shown in Fig. 1(**a3**). Figure 1(**a3**) manifests that the CPBs can suddenly focus its energy at the focal point while diffusing at the other propagation distances. Figures 1(**b**) and 1(**c**) show the intensity profiles of the CPBs by choosing the launch angles 5 and –5. The red dotted lines in Figs. 1(**a3**)–1(**c3**) display the position of the focus point with different launch angles. The numerical results show that the focal length (the distance between the input point and the maximum peak intensity point) is shortened if the CPBs exert on a positive launch angle ($v = 5$) relative to the zero launch angle ($v = 0$). On the contrary, the focal length is elongated if the CPBs are with a negative launch angle ($v = -5$). The side-view intensity profiles of the CPBs with different launch angles indicate the angle v can change the position of the focus point, and does not affect the shape and propagation trajectory of the beam. In addition, we defined IMAX in this article to describe the peak intensity contrast (defined as I_M/I_0, I_M is the peak intensity in the process of transmission, I_0 is the peak intensity of initial plane), which can help us learn

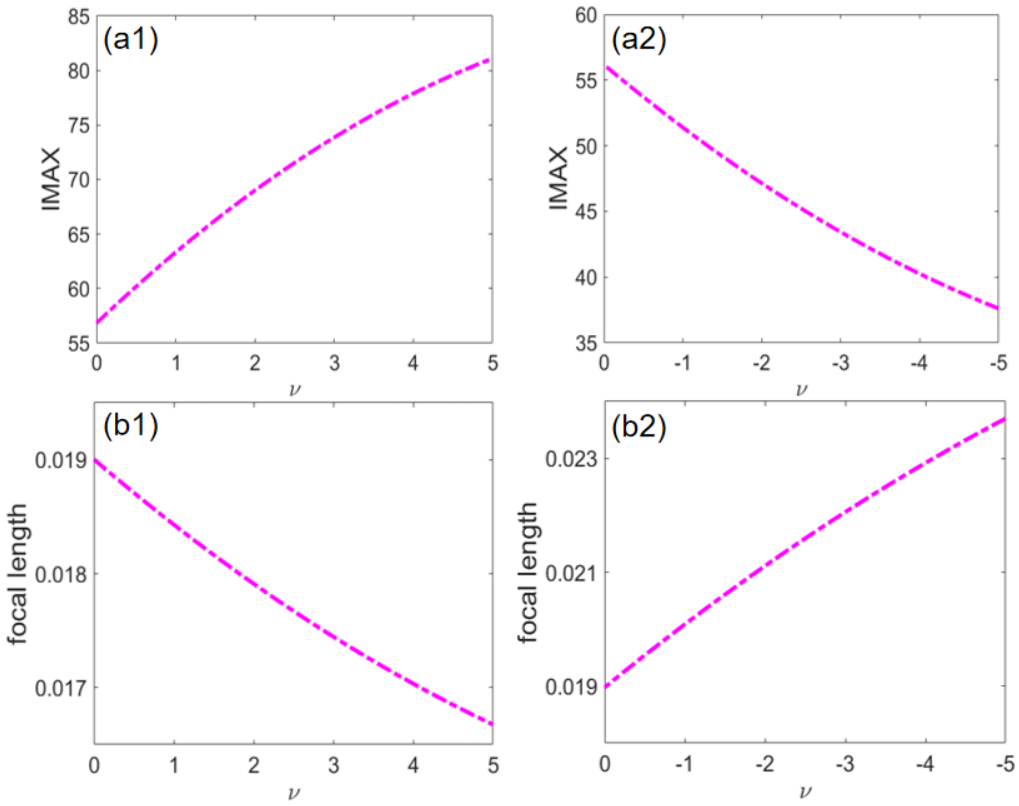

Fig. 2. The value of IMAX and focal length for different launch angles (**a1**)–(**b1**) $v > 0$, (**a2**)–(**b2**) $v < 0$.

about the properties of the CPBs. The evolution of IMAX at different propagation distances with different launch angles is shown in Fig. 1(**d1**). The intensity of the beam suddenly increases near the focus point, and decreases rapidly away from the focus point, showing the nature of sudden focusing. In general, the curve of intensity has the form of a parabola. From Fig. 1(**d1**), we can observe that different focus points are located at $z = 0.019, 0.017, 0.023$ for $v = 0$, 5 and –5, respectively. The simulation results are consistent with the above conclusion about the focal length from Figs. 1(**a3**)–1(**c3**). In addition, Figure 1(**d1**) shows that the value of IMAX is 57, 81 and 37 for $v = 0$, 5 and –5, respectively. The value of IMAX increases by choosing a launch angle $v = 5$ relative to the zero launch angle, and *vice versa*. The three-dimensional maps of the CPBs with different launch angles v are depicted in Figs. 1(**d2**)–1(**d3**).

In order to manifest the trend of intensity curve under the action of different angles *v*, we calculate the analytical trajectories of the peak intensity contrast of the CPBs as shown in Fig. 2(**a**). The curve indicates that positive launch angles can vastly increase the peak intensity contrast while negative launch angles do the opposite action. Simultaneously, we also present the function of focal length *versus* positive launch angles and negative launch angles as shown in Fig. 2(**b**). The simulation results manifest that

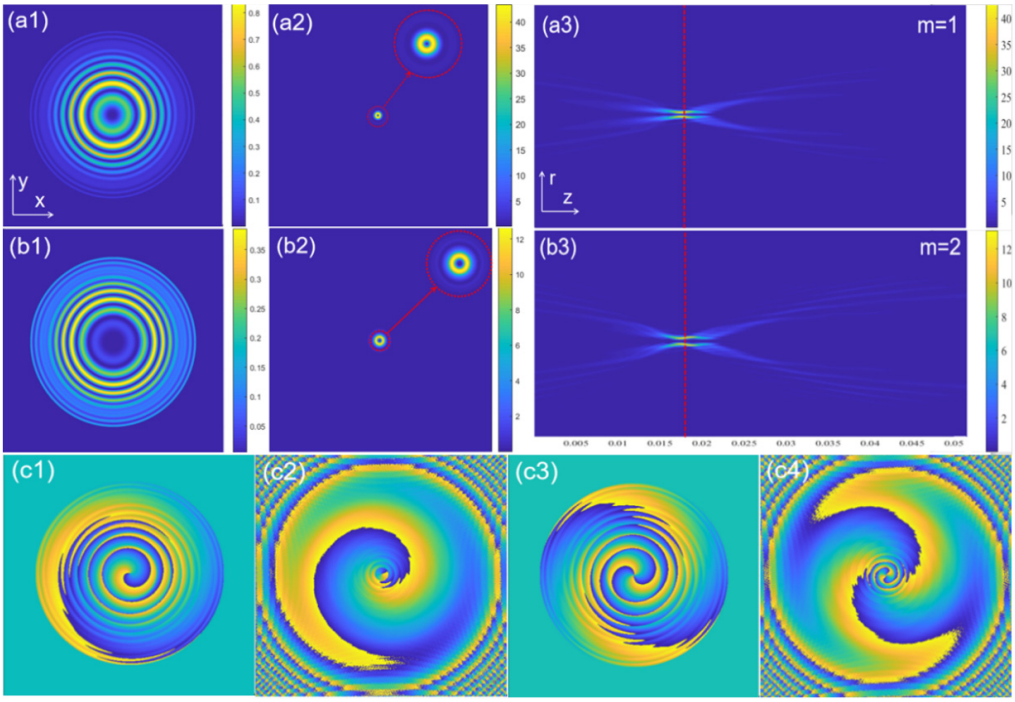

Fig. 3. The evolution of the CPVBs for different topological charges $m = 1$ and $m = 2$ in the process of transmission. (**a1**)–(**b1**) the shape and intensity distribution of the initial plane. (**a2**)–(**b2**) the shape and intensity distribution of the focal plane. (**a3**)–(**b3**) are the side-view patterns of the CPVB for $m = 1$ and 2, respectively. (**c1**) and (**c3**) represent the phase pattern at the initial plane for $m = 1$ and 2, respectively. (**c2**) and (**c3**) represent the phase pattern at the focal plane for $m = 1$ and 2, respectively.

the focal length curve increases or decreases monotonously. According to the above discussions, we can modulate the peak intensity contrast and the focal length by varying the launch angle v of the CPBs.

3.2. Propagation characteristics of the circular Pearcey vortex beams

In the previous part, we have discussed how different launch angles affect the properties of the CPBs. Now, we consider another situation – the CPBs with vortex. The evolution of the CPVBs with different topological charges under a fixed launch angle $v = 5$ has been investigated as shown in Fig. 3. Figure 3(**a**) describes the initial plane, the focal plane and the side-view intensity profile when the topological charge is set as 1.

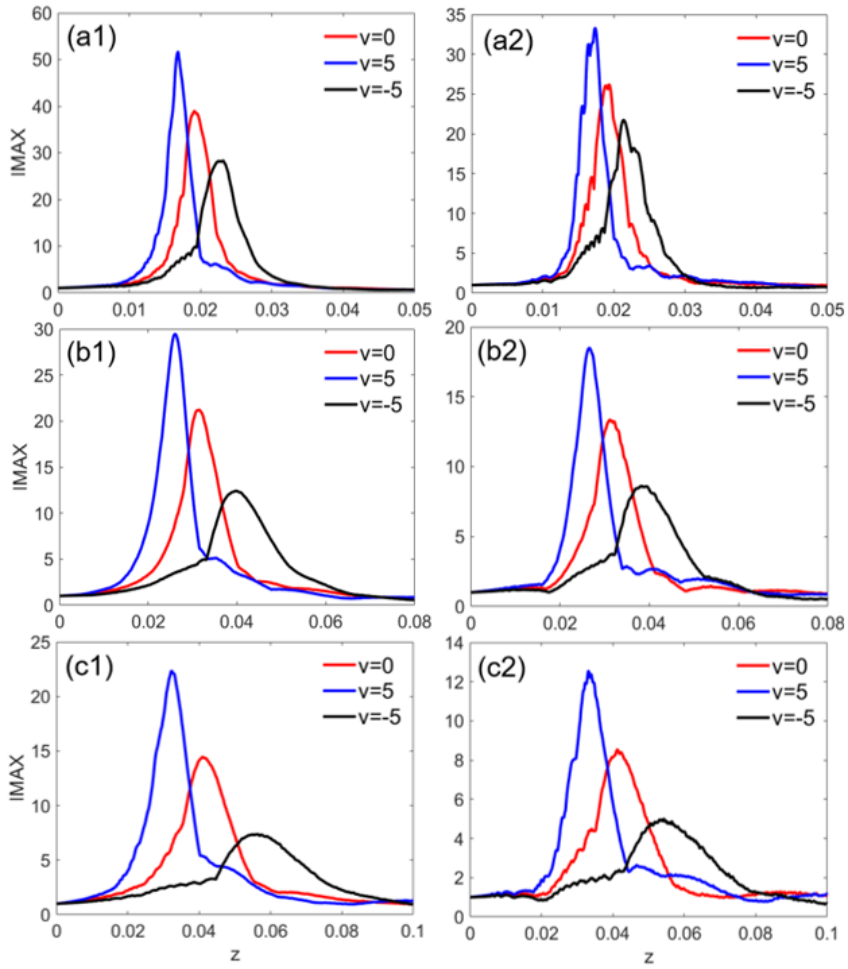

Fig. 4. The intensity distributions and the focal position of the CPVBs *versus* the propagation distance with different initial launch angles: left column (**a1**)–(**c1**) $m = 1$, right column, (**a2**)–(**c2**) $m = 2$. Different distribution factors μ: (**a**) $\mu = 0.1$ (**b**) $\mu = 0.13$, and (**c**) $\mu = 0.15$.

Compared with Fig. 1(**b**), the light intensity at the central domain is zero due to vortex on-axis. Unlike the CPBs, the side-view intensity profiles of the CPVBs display the hollow region in the central domain. Those attractive properties can be used to trap and guide the microparticle along the prospective pathway. It should be noted that the position of the maximum energy circle is concentrated in the second ring and third ring by choosing different topological charges as shown in Fig. 3(**a1**) and Fig. 3(**b1**). The hollow region becomes larger when adding the magnitude of topological charges. However, the existence of topological charges merely changes focal pattern and peak intensity contrast, the focal length of the CPVBs keeps unchanged ($z = 0.017$). Compared with phase distribution of the initial plane by choosing topological charges $m = 1$ and $m = 2$, the phase distribution of the CPVBs behaves totally spiral and begins to rotate with respect to the center taken as the starting point, except different appearance.

Next, we will discuss how different spatial distribution factor μ affects the peak intensity contrast and the focal length of the CPVBs. The left column of Fig. 4 (*i.e.*, Figs. 4(**a1**), 4(**b1**), 4(**c1**)) shows the influence of the distribution factor μ on the IMAX as well as the focal length of the CPVBs under different launch angles v by choosing the topological charge $m = 1$. The left column reveals that the spatial distribution factor μ

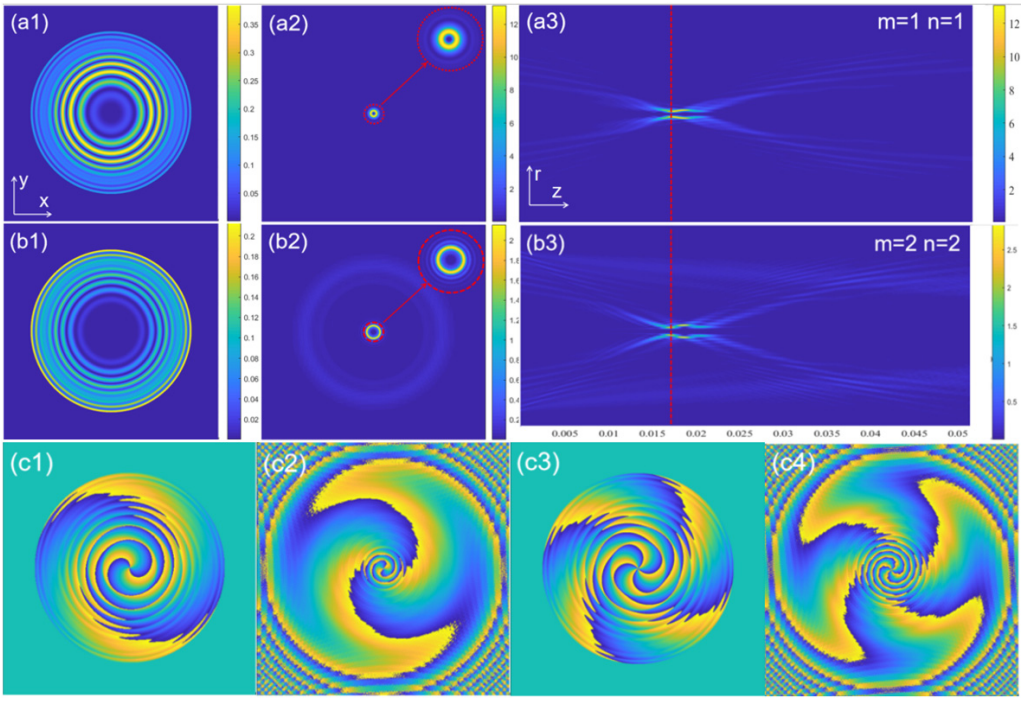

Fig. 5. The evolution of the CPVBs with two opposite vortexes. (**a1**)–(**b1**) the shape and intensity distribution of the initial plane. (**a2**)-(**b2**) the shape and intensity distribution of the focal plane. (**a3**)–(**b3**) side-view pattern of the CPVBs for different topological charges. (**c1**) and (**c3**) represent the phase pattern at the initial plane for ($m = 1$, $n = 1$), ($m = 2$, $n = 2$), respectively. (**c2**) and (**c3**) represent the phase pattern at the focal plane for ($m = 1$, $n = 1$), ($m = 2$, $n = 2$), respectively.

greatly influences the focal intensity and focal length: the larger μ, the larger focal length, but smaller IMAX. Similar conclusion can be obtained for the CPVBs with a larger topological charge parameter $m = 2$ (right column of Fig. 4). The left column and right column show that different topological charges can affect the peak intensity contrast. Obviously, the maximum value of IMAX under the action of topological charges $m = 1$ is greater than the other one. However, the position of the focus point is not distinctly changed.

3.3. The propagation properties of the CPVBs with two opposite OVs

Figure 5 shows the propagation characteristics of the CPVBs with two opposite vortexes under a fixed modulated angle $v = 5$. The intensity distribution of the initial plane by choosing topological charges $m = 1$, $n = 1$ is concentrated in the third and fourth concentric ring as shown in Fig. 5(**a1**). By increasing the value of topological charges ($m = 2$, $n = 2$), the energy of the CPVBs concentrates again in the outer circle and the dark core area becomes larger. The change of topological charges only adjusts the peak intensity contrast of the CPVBs, which is consistent with the conclusion of the CPVBs by imposing single vortex. The corresponding phase distribution of the CPVBs is shown in Figs. 5(**c1**)–5(**c3**).

Finally, to understand vortices deeply, in this paper, we demonstrate the properties of the CPVBs by altering the position of vortex. Figure 6 depicts the intensity profile of the CPVBs with different φ_k at different propagation distances. Compared to Fig. 5(**a1**), the structure of the initial plane is symmetrical but not concentric rings. CPVBs will abruptly focus and rotate at a certain angle (about 90 degrees) where the transmission distance arrives at the focus position as shown in Fig. 6(**a3**). The evolution of the CPVBs

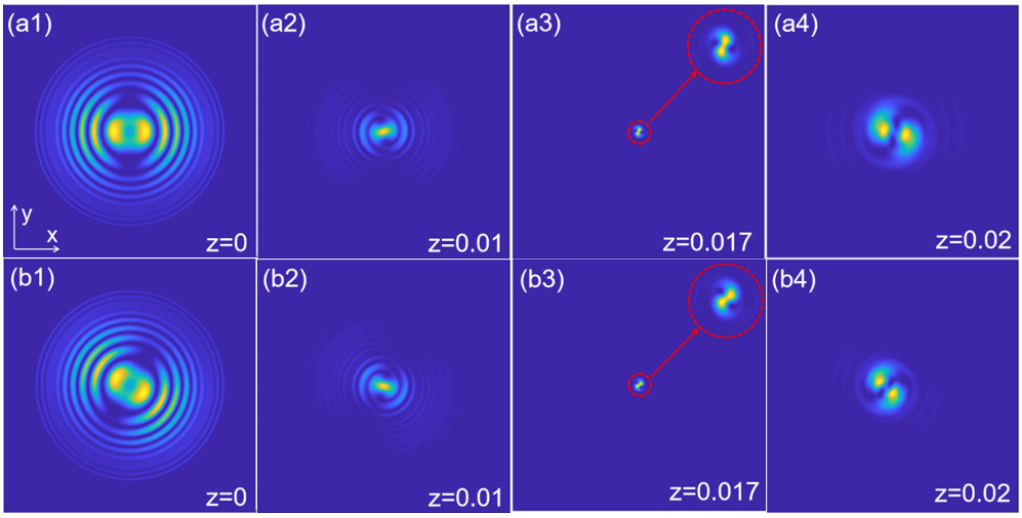

Fig. 6. The shape and intensity distribution of the CPVBs at different propagation distances: (**a1**)–(**a3**) $\varphi_k = \pi/2$. (**b1**)–(**b3**) $\varphi_k = \pi/3$. Other parameters: $m = 1$, $n = 1$, $v = 5$, and $k = 0.5$.

by choosing different vortex positions ($\varphi_k = \pi/3$) is shown in Fig. 6(**b**). The intensity distribution of the CPVBs shifts and repeats the previous rotation during propagation.

4. Conclusion

In summary, we have explored the evolution of the CPBs by adding different launch angles analytically and numerically. The focal length of the CPBs is proportional to the launch angle and the value of IMAX is inversely proportional to the launch angle. Meanwhile, adjusting the magnitude of topological charges as well as the position of vortex can alter the peak intensity contrast and focal pattern. The intensity distribution of the CPVBs shows that the central energy of the beam is zero and has a dark hollow shape. Furthermore, we also discussed the propagation of the CPVBs under the action of double opposite optical vortices. By considering the vortex and initial launch angles one can change focal pattern, focal length and peak intensity contrast, which is a momentous work in the optic media. We believe the circular Pearcey vortex beams under different angles can extend research on abruptly autofocusing beams.

Funding

The work was supported by the National Natural Science Foundation of China (Gran Nos. 61705159, 51303165 and 61705157); The Natural Science Foundation of Shanxi Province (Grant Nos. 202103021224090, 201801D121135); Shanxi "1331 Project" Key Innovative Research Team. The Special/Youth Foundation of Taiyuan University of Technology (Grant No. tyutrc201387a).

References

[1] EFREMIDIS N.K., CHRISTODOULIDES D.N., *Abruptly autofocusing waves*, Optics Letters **35**(23), 2010, pp. 4045–4047, DOI: 10.1364/OL.35.004045.

[2] PAPAZOGLOU D.G., EFREMIDIS N.K., CHRISTODOULIDES D.N., TZORTZAKIS S., *Observation of abruptly autofocusing waves*, Optics Letters **36**(10), 2011, pp. 1842–1844, DOI: 10.1364/OL.36.001842.

[3] ZHANG P., PRAKASH J., ZHANG Z., MILLS M.S., EFREMIDIS N.K., CHRISTODOULIDES D.N., CHEN Z., *Trapping and guiding microparticles with morphing autofocusing Airy beams*, Optics Letters **36**(15), 2011, pp. 2883–2885, DOI: 10.1364/OL.36.002883.

[4] MANOUSIDAKI M., PAPAZOGLOU D.G., FARSARI M., TZORTZAKIS S., *Abruptly autofocusing beams enable advanced multiscale photo-polymerization*, Optica **3**(5), 2016, pp. 525–530, DOI: 10.1364/OPTICA.3.000525.

[5] LIU K., KOULOUKLIDIS A.D., PAPAZOGLOU D.G., TZORTZAKIS S., ZHANG X.C., *Enhanced terahertz wave emission from air-plasma tailored by abruptly autofocusing laser beams*, Optica **3**(6), 2016, pp. 605–608, DOI: 10.1364/OPTICA.3.000605.

[6] SIVILOGLOU G.A., BROKY J., DOGARIU A., CHRISTODOULIDES D.N., *Observation of accelerating Airy beams*, Physical Review Letters **99**(21), 2007, 213901, DOI: 10.1103/PhysRevLett.99.213901.

[7] DURNIN J., MICELI J.J., JR., EBERLY J.H., *Diffraction-free beams*, Physical Review Letters **58**(15), 1987, pp. 1499–1501, DOI: 10.1103/PhysRevLett.58.1499.

[8] LIU F., ZHANG J.W., ZHONG W.P., BELIĆ M.R., ZHANG Y., ZHANG Y.P., LI F.L., ZHANG Y.Q., *Manipulation of Airy beams in dynamic parabolic potentials*, Annalen der Physik **532**(4), 2020, 1900583, DOI: 10.1002/andp.201900584.

[9] ZHONG H., ZHANG Y.Q., BELIĆ M.R., LI C.B., WEN F., ZHANG Z.Y., ZHANG Y.P., *Controllable circular Airy beams via dynamic linear potential*, Optics Express **24**(7), 2016, pp. 7495–7506, DOI: 10.1364/OE.24.007495.

[10] Zhang Y.Q., Belić M.R., Sun J., Zheng H.B., Wu Z.K., Chen H.X., Zhang Y.P., *Controllable acceleration and deceleration of Airy beams via an initial velocity*, Romanian Reports in Physics **67**(3), 2015, pp. 1099–1107.

[11] Zhang Y.Q., Belić M.R., Zheng H.B., Chen H.X., Li C.B., Li Y.Y., Zhang Y.P., *Interactions of Airy beams, nonlinear accelerating beams, and induced solitons in Kerr and saturable nonlinear media*, Optics Express **22**(6), 2014, pp. 7160–7171, DOI: 10.1364/OE.22.007160.

[12] Zhang Y.Q., Belić M., Wu Z.K., Zheng H.B., Lu K.Q., Li Y.Y., Zhang Y.P., *Soliton pair generation in the interactions of Airy and nonlinear accelerating beams*, Optics Letters **38**(22), 2013, pp. 4585–4588, DOI: 10.1364/OL.38.004585.

[13] Zhang J.G., Yang X.S., *Periodic abruptly autofocusing and autodefocusing behavior of circular Airy beams in parabolic optical potentials*, Optics Communications **420**, 2018, pp. 163–167, DOI: 10.1016/j.optcom.2018.03.065.

[14] Zhu Y., Zhang Y., Hu Z., *Spiral spectrum of Airy beams propagation through moderate-to-strong turbulence of maritime atmosphere*, Optics Express **24**(10), 2016, pp. 10837–10857, DOI: 10.1364/OE.24.010847.

[15] Yan X., Guo L., Cheng M.J., Li J.T., *Controlling abruptly autofocusing vortex beams to mitigate crosstalk and vortex splitting in free-space optical communication*, Optics Express **26**(10), 2018, pp. 12605–12619, DOI: 10.1364/OE.26.012605.

[16] Davis J.A., Cottrell D.M., Sand D., *Abruptly autofocusing vortex beams*, Optics Express **20**(12), 2012, pp. 13302–13310, DOI: 10.1364/OE.20.013302.

[17] Jiang Y.F., Huang K.K., Lu X.H., *Propagation dynamics of abruptly autofocusing Airy beams with optical vortices*, Optics Express **20**(17), 2012, pp. 18579–18584, DOI: 10.1364/OE.20.018579.

[18] Chen B., Chen C.D., Peng X., Peng Y.L., Zhou M.L., Deng D.M., *Propagation of sharply autofocused ring Airy Gaussian vortex beams*, Optics Express **23**(15), 2015, pp. 19288–19298, DOI: 10.1364/OE.23.019288.

[19] Ring J.D., Lindberg J., Mourka A., Mazilu M., Dholakia K., Dennis M.R., *Auto-focusing and self-healing of Pearcey beams*, Optics Express **20**(17), 2012, pp. 18955–18966, DOI: 10.1364/OE.20.018955.

[20] Deng D.M., Chen C.D., Zhao X., Chen B., Peng X., Zheng Y.S., *Virtual source of a Pearcey beam*, Optics Letters **39**(9), 2014, pp. 2703–2706, DOI: 10.1364/OL.39.002703.

[21] Kovalev A.A., Kotlyar V.V., Zaskanov S.G., Porfirev A.P., *Half Pearcey laser beams*, Journal of Optics **17**(3), 2015, 035604, DOI: 10.1088/2040-8978/17/3/035604.

[22] Chen X.Y., Deng D.M., Zhuang J.L., Peng X., Li D.D., Zhang L., Zhao F., Yang X.B., Liu H.Z., Wang G.H., *Focusing properties of circle Pearcey beams*, Optics Letters **43**(15), 2018, pp. 3626–3629, DOI: 10.1364/OL.43.003626.

[23] Chen X.Y., Deng D.M., Wang G.H., Yang X.B., Liu H.Z., *Abruptly autofocused and rotated circular chirp Pearcey Gaussian vortex beams*, Optics Letters **44**(4), 2019, pp. 955–958, DOI: 10.1364/OL.44.000955.

[24] Zhang L.P., Deng D.M., Yang X.B., Wang G.H., Liu H.Z., *Effects of the modulated vortex and second-order chirp on the propagation dynamics of ring Pearcey Gaussian beams*, Optics Letters **44**(19), 2019, pp. 4654–4657, DOI: 10.1364/OL.44.004654.

[25] Sun C., Deng D.M., Yang X.B., Wang G.H., *Propagation dynamics of autofocusing circle Pearcey Gaussian vortex beams in a harmonic potential*, Optics Express **28**(1), 2020, pp. 325–333, DOI: 10.1364/OE.28.000325.

[26] Xu C.J., Wu J.H., Wu Y., Lin L.D., Zhang J.B., Deng D.M., *Propagation of the Pearcey Gaussian beams in a medium with a parabolic refractive index*, Optics Communications **464**, 2020, 125478, DOI: 10.1016/j.optcom.2020.125478.

[27] Long X.W., He Q.L., Deng X.P., Bai J., Liu C., *Trajectory and focal length of circular Airy beams with different launch angles in linear potentials*, Optics Communications **450**, 2019, pp. 256–275, DOI: 10.1016/j.optcom.2019.06.020.

[28] ZHANG J.G., LI Y.F., TIAN Z.W., LEI D.J., *Controllable autofocusing properties of conical circular Airy beams*, Optics Communications **391**, 2017, pp. 116–120, DOI: 10.1016/j.optcom.2017.01.027.
[29] CHREMMOS I., ZHANG P., PRAKASH J., EFREMIDIS N.K., CHRISTODOULIDES D.N., CHEN Z., *Fourier-space generation of abruptly autofocusing beams and optical bottle beams*, Optics Letters **36**(18), 2011, pp. 3675–3677, DOI: 10.1364/OL.36.003675.
[30] POON T.C., KIM T., *Engineering optics with MATLAB*, Word Scientific, 2006.
[31] ZHANG Y.Q., LIU X., BELIĆ M.R., ZHONG W.P., WEN F., ZHANG Y.P., *Anharmonic propagation of two-dimensional beams carrying orbital angular momentum in a harmonic potential*, Optics Letters **40**(16), 2015, pp. 3786–3789, DOI: 10.1364/OL.40.003786.
[32] PEARCEY T., *XXXI. The structure of an electromagnetic field in the neighbourhood of a cusp of a caustic*, The London, Edinburgh, and Dublin Philosophical Magazine and Journal of Science, Series 7, Volume 37, Issue 268, 1946, pp. 311–317, DOI: 10.1080/14786444608561335.

Received July 7, 2021
in revised form November 10, 2021